Continuous monitoring of back wall stress corrosion cracking growth in sensitized type 304 stainless steel weldment by means of potential drop techniques

Continuous monitoring of back wall stress corrosion cracking growth in sensitized type 304 stainless steel weldment by means of potential drop techniques

Y. Sato [a, *], T. Atsumi [a], T. Shoji [a]

[a] Fracture and Reliability Research Institute(FRI), Tohoku University,
Aramaki Aoba6-6-01, Aoba-ku Sendai/980-8579, Japan

Abstract

Stress corrosion cracking (SCC) tests on welded specimens of sensitized type 304SS with a thickness of 20 mm were performed in sodium thiosulphate solution at room temperature, with continuous monitoring of the SCC growth, using the techniques of modified induced current potential drop (MICPD), alternating current potential drop (ACPD) and direct current potential drop (DCPD). The MICPD and DCPD techniques permit continuous monitoring of the back wall SCC, which initiates from a fatigue pre-crack at a depth of about 4mm, from which it propagates through more than 80% of the specimen thickness. The MICPD technique can decrease the effect of the current flowing in the direction of the crack length by focusing the induced current into the local area of measurement using induction coils, so that the sensitivity of the continuous monitoring of the back wall SCC is higher than that of the ACPD and DCPD techniques.

Key words; Stress corrosion cracking, Sensitized stainless steel, Continuous monitoring, Potential drop

1. Introduction

It was thought that the stress corrosion cracking (SCC) problems in boiling water reactor (BWR) plants which occurred during the 1970's [1] had been solved by employing L-grade stainless steels, which contain less carbon, to avoid the sensitization due to welding. However, recently, many cracking incidents, involving the L-grade stainless steel components, due to SCC have been discovered in BWR plants [2], and as a result, the reduction in reliability of the components and piping has led to a decline in the operational rate of the plants. In order to perform stable operation of a nuclear power plant, both high sensitivity in the detection of defects and precise sizing of the defects by periodic inspection are important. In addition, continuous monitoring of the detected cracks which remain, subject to evaluation based on maintenance standards, can result in improved reliability of the plant. Moreover, the operation rate of the plants can be

* Corresponding author. Tel.: +81-22-795-7520; fax.: +81-22-795-7543.
E-mail address: yasumoto.sato@rift.mech.tohoku.ac.jp

reasonably increased by making the intervals between periodic inspections longer, based on the continuous monitoring of defects. The techniques which will be employed for the continuous monitoring of defects should be (1) reliable, (2) accurate and sensitive, and (3) simple.

Potential drop (PD) techniques may be applicable to the continuous monitoring of defects in the plant operation environment because these techniques utilize a very simple sensor which merely consists of electrical wiring and have already been used for in-situ SCC growth monitoring in laboratories [3]. The PD techniques are divided roughly into a direct-current potential drop (DCPD) technique [4] and an alternating-current potential drop (ACPD) technique [5] according to the current utilized. One of the ACPD techniques, namely the induced current potential drop (ICPD) technique based on electromagnetic induction, has been developed [6].

In this study, in order to investigate the applicability of the PD techniques to the continuous monitoring of SCC growth, SCC tests were performed in a sodium thiosulphate solution at room temperature using plate specimens with weldments. The SCC growth was monitored using the PD techniques on the reverse side to that on which the SCC existed and the effectiveness of each technique for the continuous monitoring from the reverse side of SCC was compared from the viewpoints of sensitivity to the crack growth and measurement stability.

2. Optimization of measurement conditions for the modified induced current potential drop technique

2.1 The modified induced current potential drop technique

The PD technique used in this study is a modification of the basic PD technique based on electromagnetic induction, which has been developed mainly for both detection and sizing of surface breaking cracks [7, 8, 9]. The PD technique based on electromagnetic induction supplies an alternating current to the object under inspection using induction wires or a single coil located near the surface of the object, without direct contact, unlike the standard PD techniques in which a current is directly supplied to the object under test through electrical terminals, and measures the perturbation of the current which occurs as a result of defects. In order to apply the PD technique, based on electromagnetic induction, to the continuous monitoring of back wall SCC growth with sufficient sensitivity, we modified the PD technique using two induction coils located on each side of potential drop pick-up terminals, in order to induce a larger current around the local area of measurements than obtained with induction wires or a single coil (the modified induced current potential drop (MICPD) technique).

The MICPD technique can result in two types of sensor with respect to the

arrangement of the induction coils; a horizontal flux sensor, in which the magnetic flux generated by the two coils is parallel to the surface of the specimen (Figure 1 (a)) and a vertical flux sensor, in which the magnetic flux generated by the two coils is perpendicular to the surface of the specimen (Figure 1 (b)).

The sensitivity of the MICPD technique to back wall cracks will strongly depend on the conditions of the induced current. Accordingly, the frequency of the current and the arrangement of the two induction coils must be optimized for the measurement of back wall cracks. Initially, finite element method (FEM) analysis of the induced current distributions by these two sensors was performed, in order to confirm that the induced current is focused on the local area of measurement. Following the FEM analysis, inspections of back wall defects were performed, changing the experimental parameters to determine the measurement condition which provided the maximum sensitivity to back wall defects.

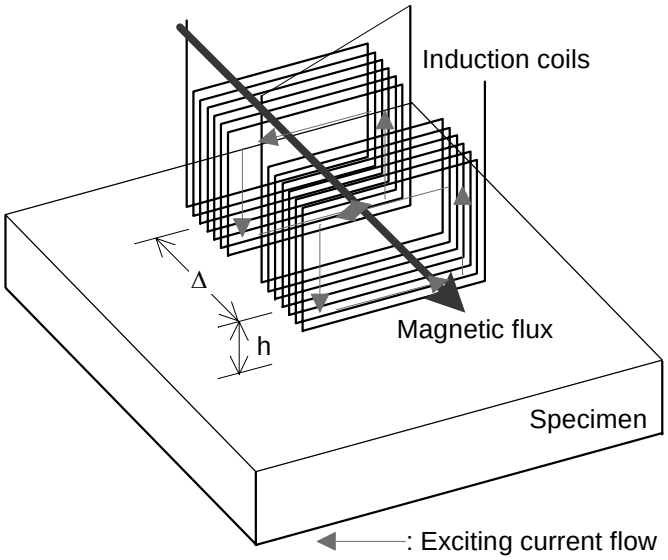

(a) Horizontal flux sensor

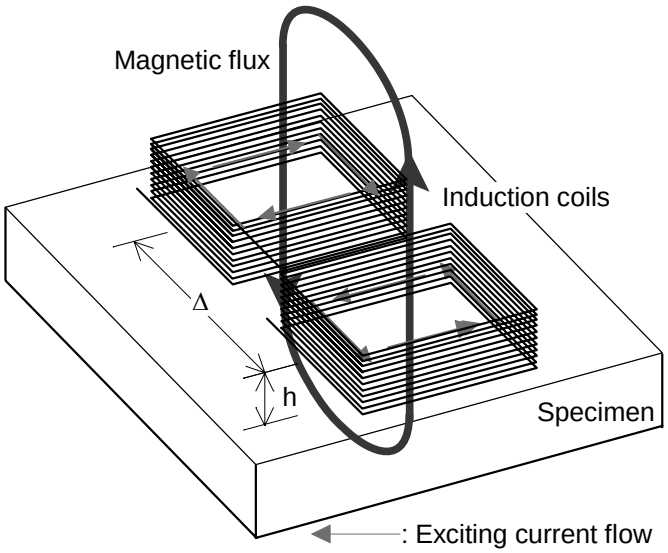

(b) Vertical flux sensor

Figure 1 Illustrations of the arrangement of induction coils.

2.2 Sensors, specimen and measurement procedures

A schematic illustration of the developed vertical flux sensor is shown in Figure 2. The sensor has a pair of induction coils to induce a current in the object to be measured and a pair of electrical terminals to measure the potential drop. The distance between the two terminals is 5mm. The induction coil is a 58 turn rectangular coil, with a length of 60mm, a width of 30mm and a height of 15mm. The horizontal flux sensor uses the same induction coils as above, but with a different orientation.

The specimen used for the inspection was a plate of type 316 stainless steel (316SS), containing two rectangular electrical discharge machined (EDM) slits with a length of 10mm, a width of 0.5mm and depths of 1 and 3mm.

Measurement parameters investigated in this study for the vertical flux sensor were current frequencies of 1 and 0.3kHz, and distances between the two induction coils (Δ) of 70 and 100mm, whilst for the horizontal flux sensor, the distances between the bottom of the induction coils and the specimen (H) were 0 and 30mm, and the distances between the two induction coils (Δ) were 35, 65 and 95mm. The excitation current was fixed at 2A. Combinations of measurement parameters investigated for each sensor are summarized in Table 1.

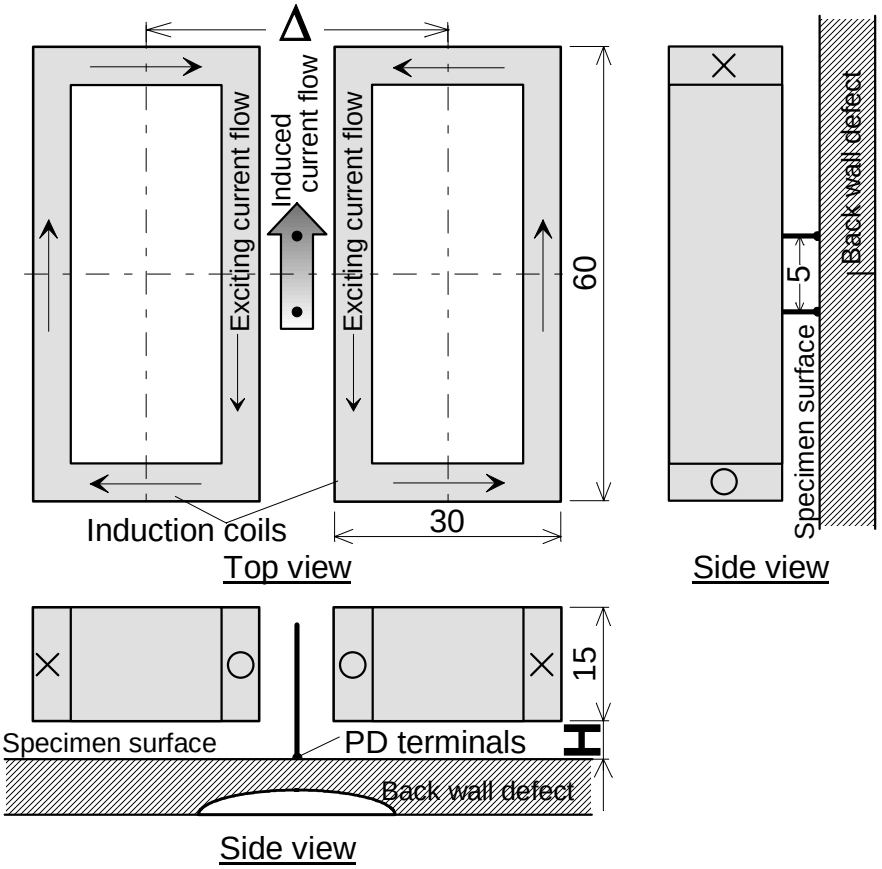

Figure 2 Illustration of the vertical flux sensor (dimensions in mm).

Table 1 Combinations of measurement parameters for each sensor.
(Excitation current was fixed to 2A)

(a) Vertical flux sensor (H was fixed 5mm)

Current frequency , Hz	Δ , mm
0.3	70
	100
1.0	70
	100

(b) Horizontal flux sensor (Current frequency was fixed at 0.3kHz)

H , mm	Δ , mm
0	35
	65
	95
30	35
	65

2.3 FEM analysis of induced current density

2.3.1 FEM model

The current distributions, induced by the MICPD sensors, were calculated by FEM analysis, prior to the fabrication of the sensors.

A schematic illustration of the model investigated with FEM analysis is shown in Figure 3. The model contains the specimen (316SS), induction coils (Copper) and air surrounding the specimen and coils. The electromagnetic properties used for the FEM analysis are summarized in Table 2.

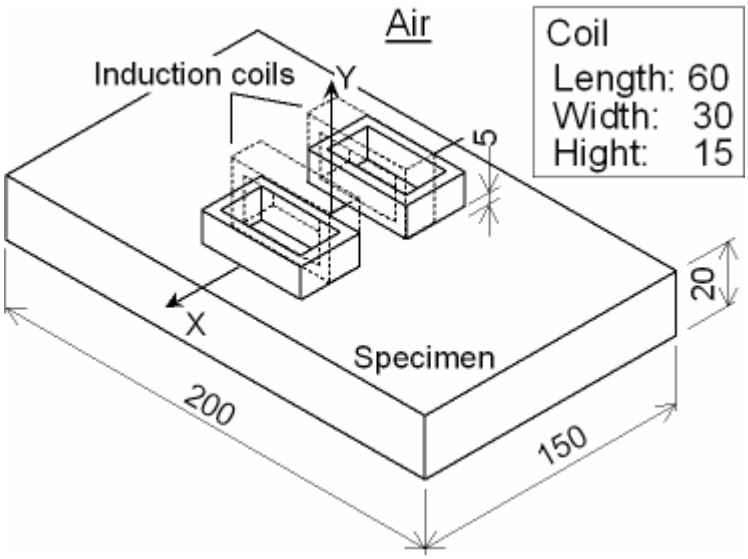

Figure 3 Illustration of the model for the FEM analysis (dimensions in mm).

Table 2 Electromagnetic properties used in the FEM analysis.

	Relative permeability	Electrical resistivity
Specimen (316SS)	1.003	$74.0 \times 10^{-8}\ \Omega m$
Coil (Copper)	1.000	-
Air	1.000	-

2.3.2 Induced current density distributions calculated with FEM

Current density distributions in the specimen along the X-axis, calculated with FEM, are shown in Figure 4. For the vertical flux sensor, the maximum current density is found to be at the centre, between the two induction coils. However, for the horizontal flux

sensor, the maximum current density is found to be at the edge of the specimen, with the peak current density observed just under the induction coil, decreasing to 26% as it approaches the centre, between the two induction coils. The current density at the centre, between the two induction coils for the vertical flux sensor is 4.6 times greater than that for the horizontal flux sensor.

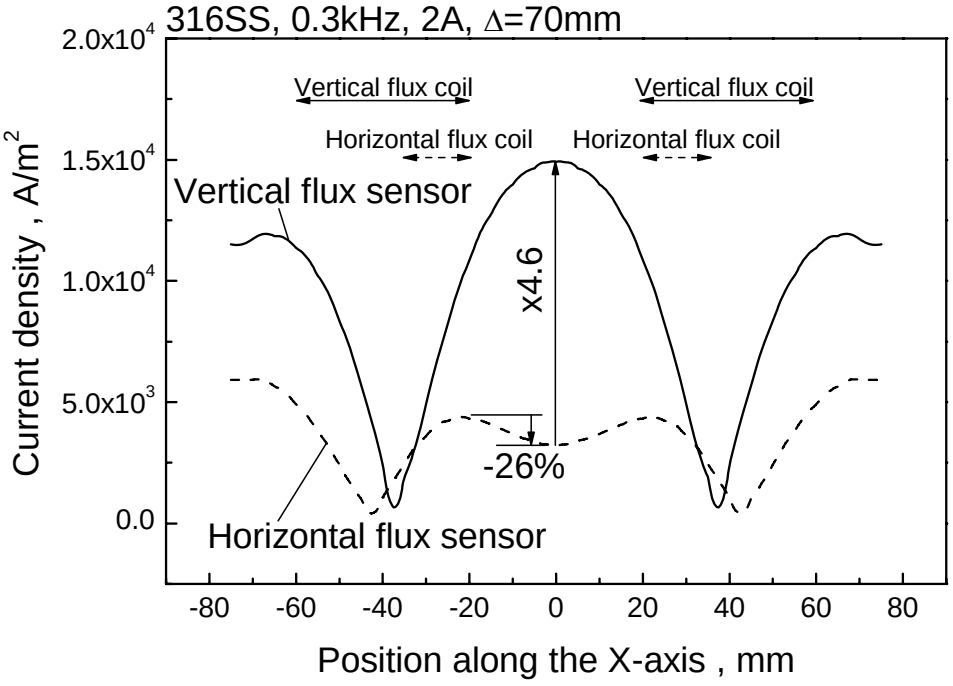

Figure 4 Current density distributions along the X-axis calculated with FEM (Δ=70mm).

2.4 Results of back wall defect inspections

Potential drop distributions measured on the 316SS plate specimen with the sensors under different measurement conditions are shown in Figure 5, as typical examples. The horizontal axis shows the position of the centre, between the two electrical terminals, for PD measurement, whilst the vertical axis indicates the normalized potential drop (NPD), which represents the ratio of the measured potential drop to the average potential drop of an intact region. There are EDM slits with depths of 1mm and 3mm at the sensor positions of 20mm and 80mm, respectively, and large NPDs are obtained around these positions. Accordingly, the large NPDs result from the existence of back wall defects. Figure 5 shows that the nature of the NPD distributions obtained from both the vertical flux and the horizontal flux sensors are similar. Although the structures are similar, it can be seen from the Figure 5 that the scattering of NPD distributions with measurement conditions for the vertical flux sensor is smaller than that for the horizontal flux sensor. Further, it was impossible to detect an EDM slit at a depth of 1mm with several of the

measurement conditions, using the horizontal flux sensor.

In this study, we defined the detection sensitivity for both the vertical and horizontal flux sensors as the ratio of the maximum NPD change, measured just above the slit, to the standard deviation in NPD of an intact region. Calculated detection sensitivities for both the vertical and horizontal flux sensors are summarized in Table 3. The EDM slit with a depth of 3mm was detected at all of the measurement conditions, except for the horizontal flux sensor with Δ of 95mm and H of 30. Hence, we have compared the detection sensitivity of each measurement condition for an EDM slit with a depth of 1mm. According to Table 3, the maximum detection sensitivity of 1.60 for the vertical flux sensor with Δ of 70 is slightly larger than that of 1.17 obtained for the horizontal flux sensor with Δ of 35mm and H of 0mm. As mentioned above, the scatter in the NPD distribution amongst measurement conditions for the horizontal flux sensor is relatively greater than that with the vertical flux sensor, implying that the detection sensitivity for the horizontal flux sensor strongly depends on the experimental set up. Further, the distance between the specimen surface and induction coils will be changed due to the bending strain during the SCC test under the load of a four point bending moment. Correspondingly, the horizontal flux sensor, whose detection sensitivity exhibits a considerable decrease due to changes in the distance between the specimen surface and the induction coils, is not suitable for the monitoring of SCCs created under a four point bending moment. We concluded therefore that the vertical flux sensor with Δ of 70mm was the most suitable for the monitoring of SCCs created under a four point bending moment.

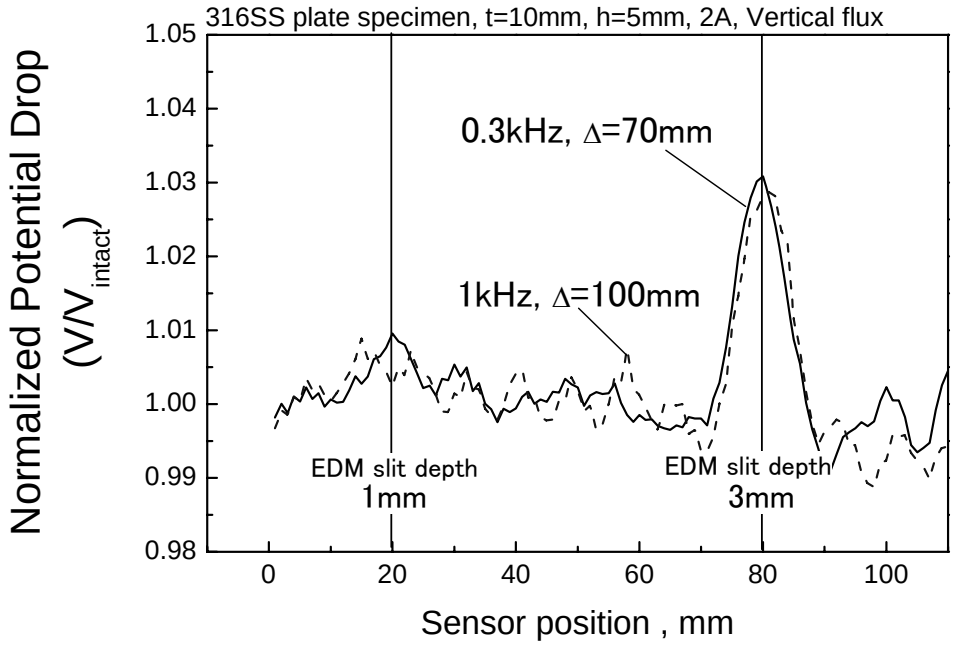

(a) Vertical flux sensor

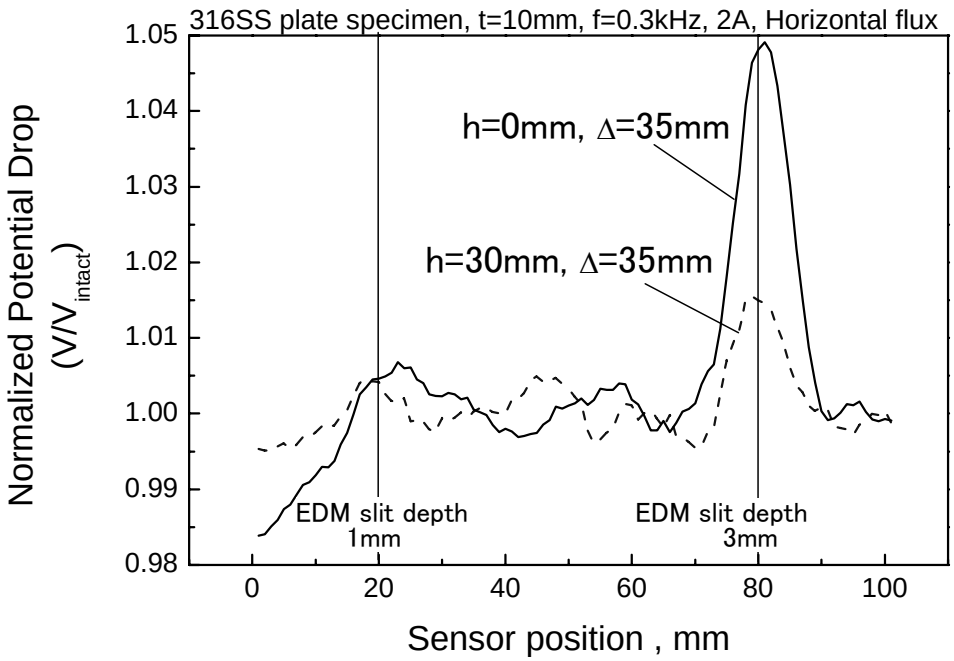

(b) Horizontal flux sensor

Figure 5 Potential drop distributions measured on the 316SS plate specimen.

Table 3 Detection sensitivity to back wall defects.

(a) Vertical flux sensor

Current frequency , kHz	Δ=70mm		Δ=100mm	
	Crack depth , mm		Crack depth , mm	
	1.0	3.0	1.0	3.0
0.3	1.60	5.86	0.12	4.71
1.0	1.34	5.91	-	4.90

(b) Horizontal flux sensor

H , mm	Δ=35mm		Δ=65mm		Δ=95mm	
	Crack depth , mm		Crack depth , mm		Crack depth , mm	
	1.0	3.0	1.0	3.0	1.0	3.0
0	1.17	9.59	-	5.48	-	8.03
30	0.65	4.33	-	4.84	-	-

3. Monitoring of SCC growth with PD techniques

3.1 Specimen and measurement system

The material used for the SCC tests was a type 304 stainless steel (304SS). The

composition and mechanical properties of the material at room temperature are shown in Table 4. A plate with the thickness of 20mm was machined from the material and butt-welded using tungsten inert gas (TIG) welding. The welding conditions are summarized in Table 5. An electro-discharge machined (EDM) slit with a depth of 2mm, a length of 10mm and a width of 0.2mm, was machined in the heat-affected zone (HAZ) of the welded plate. The EDM slit possessed a semi-elliptical shape. A schematic of the specimen used in the SCC test is shown in Figure 6.

In order to investigate the degree of sensitization to SCCs resulting from the TIG welding, measurements using the electrochemical polarization reactivation (EPR) technique [10] were performed on a small piece (10 mm X 10 mm X 2 mm) of the specimen for the SCC test. The measured EPR value for the HAZ was 1.6% and that for the parent material was 0.0%, revealing that the HAZ was almost not sensitized by the TIG welding under the conditions shown in Table 5. Accordingly, the specimens for the SCC tests were heat treated for sensitization at 650°C and 24 hours.

A schematic of the continuous monitoring system for SCCs using both the ACPD and MICPD techniques is shown in Figure 7. Although the measurement system for the DCPD technique does not contain a phase detector, the DCPD system is similar to that shown in Figure 7. The PD sensor was located on the reverse of the surface on which the crack existed.

Continuous monitoring of the SCC growth was performed, using the MICPD technique with the vertical flux sensor, under the optimized conditions found above. The electrical terminals for the PD measurement were spot welded to the surface of the specimen in order to minimize the effects of contact resistance. Continuous monitoring was also performed using the ACPD and DCPD techniques. The distance between the electrical terminals for the potential drop measurement in both the ACPD and DCPD techniques was 5 mm. The input current was 2A (0.3 kHz) for the ACPD technique and 5A for the DCPD technique. The distance between the electrical terminals for current supply was 110 mm in both the ACPD and DCPD cases.

The SCC tests were performed under the same testing conditions, using a different specimen for each PD technique.

Table 4 Chemical composition (wt%) and mechanical properties (room temperature) of the investigated 304SS.

C	Si	Mn	P	S	Cr	Ni	0.2% Proof stress	Tensile strength	Elongation
0.05	0.38	0.83	0.027	0.003	18.11	8.05	266MPa	637MPa	62%

Table 5 TIG welding conditions used for the SCC test specimens.

Welding speed	100 mm/min
Welding current	190A (11V)
Filler wire	308L SS, ϕ1.2 mm, 8.4 g/min
Groove	U-groove, Root face: 0.8 mm

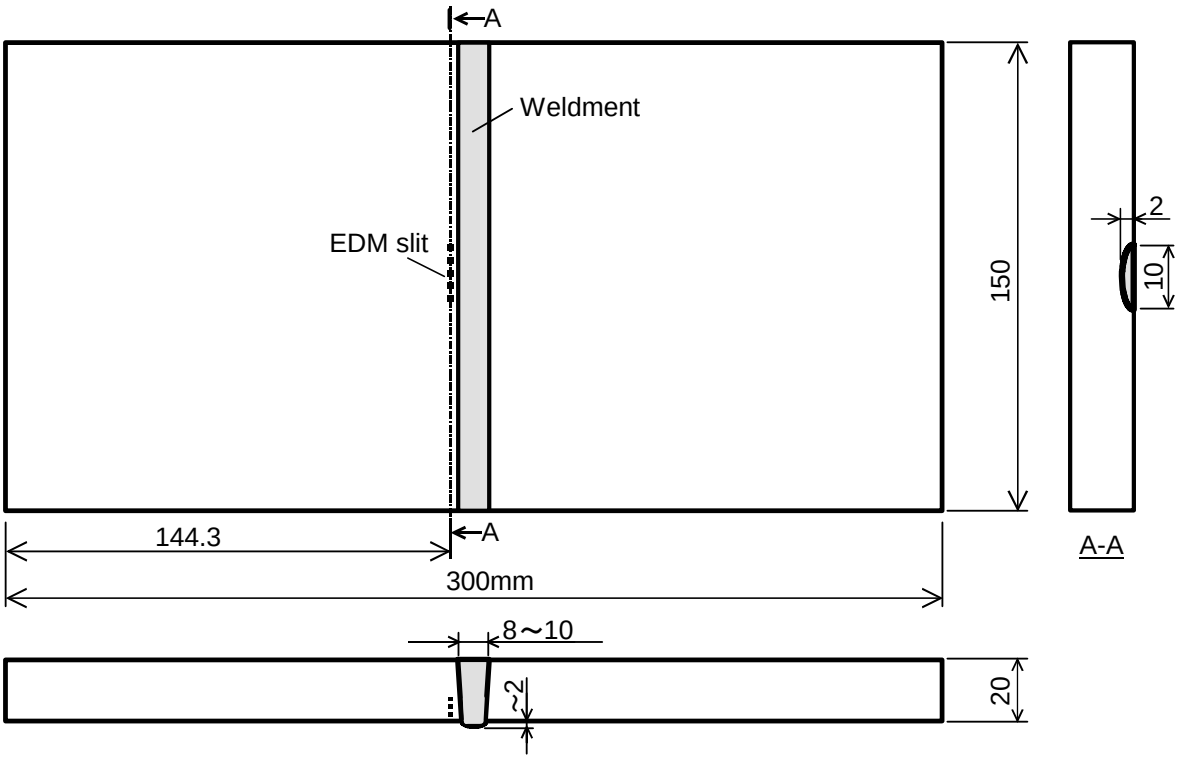

Figure 6 Specimen geometry (dimensions in mm).

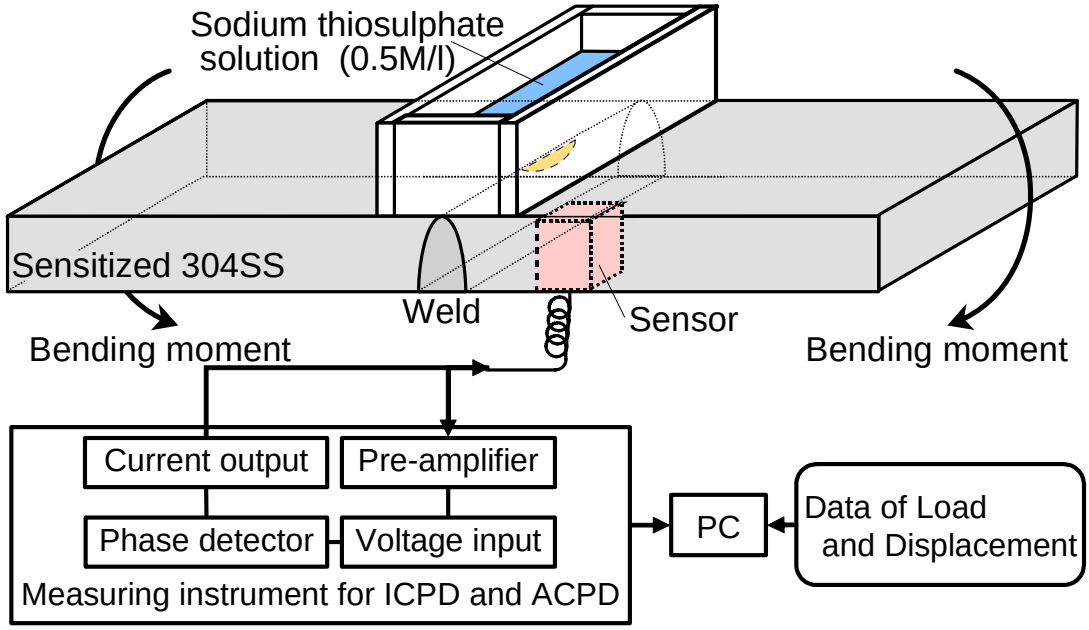

Figure 7 Illustration of the continuous monitoring system for both the ACPD and MICPD techniques.

3.2 Experimental conditions for fatigue pre-cracking and the SCC tests

The specimen was pre-cracked by fatiguing in air, prior to the SCC testing. The fatigue pre-crack was generated at a maximum stress intensity factor (K) of 16.6~17.0 $MPam^{1/2}$. The fatigue pre-cracking was performed until the estimated crack tip extended to about 4mm from the specimen surface, based on the literature crack growth rate data of 3×10^{-8} m/cycle [11]. The K value was calculated using Newman-Raju's equation [12].

After pre-cracking, the specimen was subjected to the SCC test in the sodium thiosulphate solution (0.5Mol/l) [13, 14] and the SCC growth was monitored using the PD techniques. The SCC test was performed under trapezoidal wave loading. The hold time was 9000 seconds, the unloading time was 500 seconds, and the reloading time was 500 seconds, with an unloading ratio of 0.7 (R=0.7). At the beginning of the SCC test, the target maximum K value at the crack tip was about 20 $MPam^{1/2}$. A schematic of the loading mode is shown in Figure 8. The SCC tests were terminated when the predicted crack depth, based on the surface observation, extended to greater than 75% of the specimen thickness.

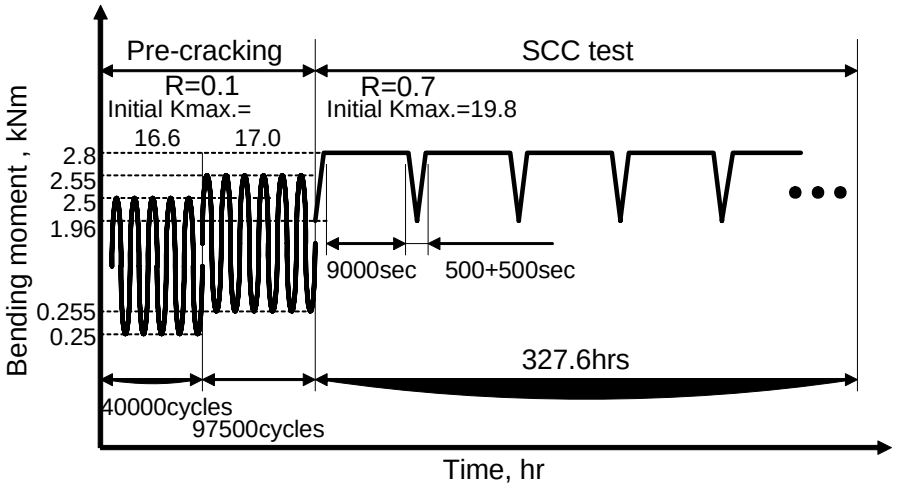

Figure 8 The mode of load application for pre-cracking and the SCC test.

3.3 Results and discussion

3.3.1 Potential drop distributions measured during the fatigue pre-cracking

Potential drop distributions measured by the PD techniques during fatigue pre-cracking are shown in Figure 9. The horizontal axis gives the loading cycle, normalized by the total numbers of cycles. Although the PDs, measured using either the DCPD or ACPD techniques show no changes, the PDs measured using the MICPD technique increase from a normalized loading cycle of 0.5. The detectable crack depth prediction, based on the loading cycle, is 3mm (15% of the specimen thickness).

3.3.2 Fracture surface

After the SCC test, the specimens were opened by fatigue cracking in air and examined using an optical microscope and by scanning electron microscopy (SEM). Fracture surfaces with typical intergranular (IG) SCC fractures of the specimen used for measurement by the MICPD technique are shown in Figure 10. The entire fracture surface created in the environment displayed an IG character. According to Figure 10, the maximum crack depths for the fatigue pre-crack and for the SCC are 4.3mm (21.5% of the specimen thickness) and 16.2mm (81.0% of the specimen thickness), respectively. As summarized in Table 6, the sizes of IGSCCs created by each SCC test are almost the same.

3.3.3 Potential drop distributions measured during the SCC test

Prior to the SCC tests, the stability of the PD readings for each PD technique was investigated. Table 7 shows the average value and the standard deviation of the PD, measured every 30 seconds over 10 hours by each of the three PD techniques. Although the average PD value with the MICPD technique is several tens times larger than those for

the ACPD and DCPD techniques, the standard deviation for the MICPD technique is similar to those of the ACPD and DCPD techniques. Thus, the MICPD technique could perform more precise measurements than the ACPD or DCPD techniques.

Changes in the PD measured with each of the PD techniques during the SCC tests are plotted in Figure 11. The horizontal axis shows the SCC testing time, normalized to the total SCC testing time. As shown in Table 6, the magnitudes for the three SCCs measured by the fracture surface observations are almost the same and, therefore, the magnitudes of the three SCCs might be similar at each normalized testing time. The vertical axis of Figure 11 shows the PD change, normalized to the total PD increment, measured until the SCC tests were terminated (Normalized potential drop change). The SCC initiations for the three SCC tests were confirmed by visual observation, just after each SCC test commenced.

From the beginning of the SCC test, the PD change from both the MICPD and DCPD techniques begins to increase as the normalized testing time increases, and the PD change continues to increase until the end of the test. During the test time period from 0.2 to 0.9, the increasing rate in the PD change obtained from the MICPD technique is greater than that obtained from the DCPD technique. In the case of the ACPD technique, it is difficult to identify the SCC growth from the beginning of the SCC test to the normalized testing time of about 0.3, due to significant scatter in the PD measurements, and later, although several PD changes exhibit very small values, the PD change increases until the end of the SCC tests at a similar rate of increase as in the DCPD technique. Summarizing these results, the sensitivity of the MICPD technique for the back wall SCC growth is greater than that of the DCPD or ACPD techniques.

The reason why the MICPD technique showed a better rate of increase in the PD change than seen with the ACPD or DCPD techniques could be attributed to the changes in the current flow due to the existence of cracks. When the electrical current flows in a direction perpendicular to the crack wall, not all of the current will flow in the direction of the crack depth, but some fraction of the current will flow in the direction of the crack length. However, the fraction of the induced current flowing in the direction of the crack length might be relatively small, compared to the current used in the ACPD or DCPD techniques, because the induced current is focused by the induction coils on the local area of measurement. The effect of the current flowing in the direction of the crack length was investigated by FEM analysis for the MICPD and ACPD techniques using the model containing two-dimensional back wall slits with depths of 7, 10 and 13mm. The ideal potential drop must be calculated by the FEM analysis because all of the current must flow in the direction of the crack depth for a two-dimensional slit. The calculated PD changes with the MICPD and ACPD techniques for a two-dimensional slit are plotted in Figure 11.

The depths of the two-dimensional slits were converted into normalized test time by calculating the ratio to the final SCC crack depth of 16mm. There is very little difference between the FEM results for the MICPD and ACPD techniques because all of the current must flow in the direction of the crack depth for the two-dimensional slit. The current reduction from the results of the FEM analysis confirms the effect of the current flowing in the direction of the crack length. The experimental results from the MICPD technique are in good agreement with the FEM results in the initial 25% of the SCC test time. However, the experimental result with the ACPD technique, for example, at the normalized test time of 0.25, has a magnitude almost half that of the FEM result and the difference between the experimental and the FEM results becomes greater as the normalized test time increases. Although the experimental results from the MICPD technique match the FEM results up to a normalized test time of 0.25, the extent of the deviation from the FEM results is 1/2 to 1/3 of that seen with the ACPD technique. Correspondingly, the higher sensitivity of the MICPD technique for the continuous monitoring of the back wall crack can be attributed to the fact that the MICPD technique can decrease the effect of the current flow in the direction of the crack length by focusing the induced current into the local area of measurement using the induction coils.

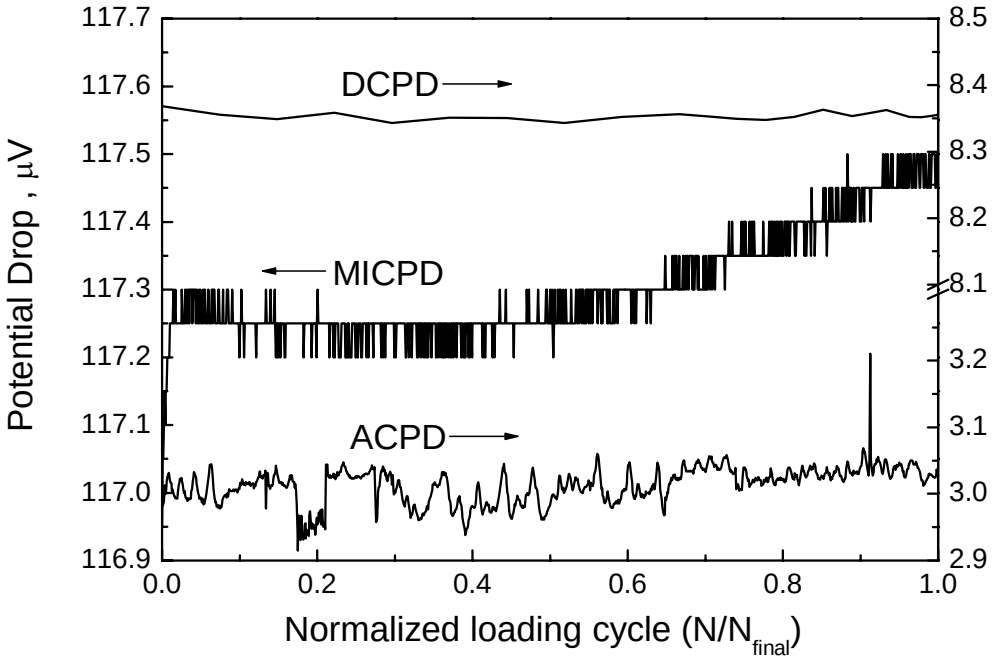

Figure 9 Potential drop distribution measured during the fatigue pre-cracking.

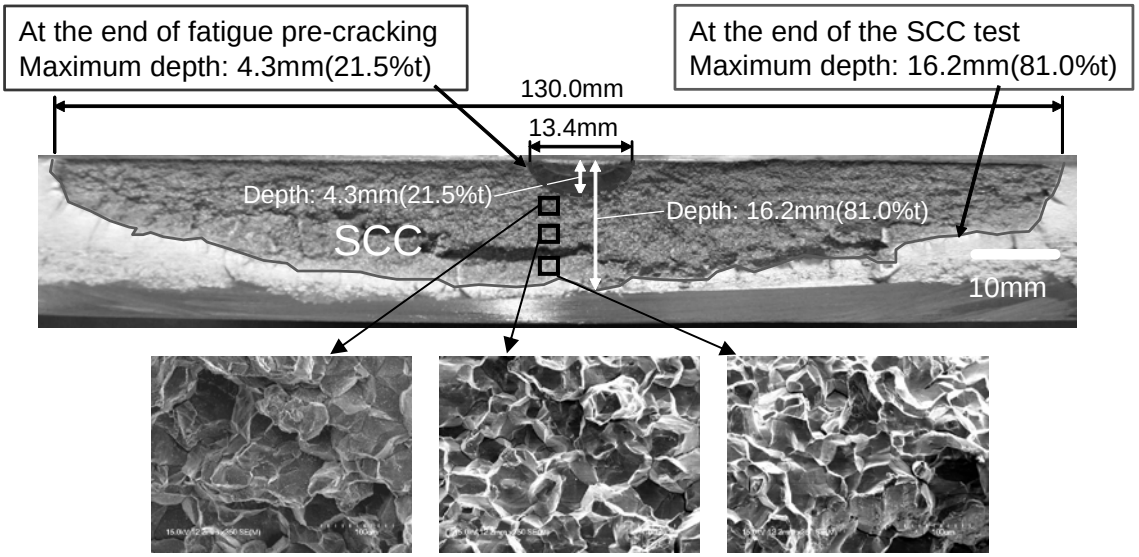

Figure 10 Fracture surface with typical IGSCC fractures for the specimen used in the measurements with the MICPD technique.

Table 6 Crack sizes for each test.

Test	Fatigue pre-crack		SCC	
	Length , mm	Depth , mm	Length , mm	Depth , mm
1 (MICPD)	13.4	4.3 (21.5%t)	130.0	16.2 (81.0%t)
2 (ACPD)	14.0	4.0 (20.0%t)	126.5	15.5 (77.5%t)
3 (DCPD)	13.5	4.0 (20.0%t)	119.5	16.0 (80.0%t)

Table 7 Measured potential drop without loading condition.

	MICPD	ACPD	DCPD
Standard deviation (SD), μV	0.023	0.015	0.018
Average PD (Avg. PD), μV	156.7	3.1	8.4
SD/Avg. PD	0.01	0.47	0.21

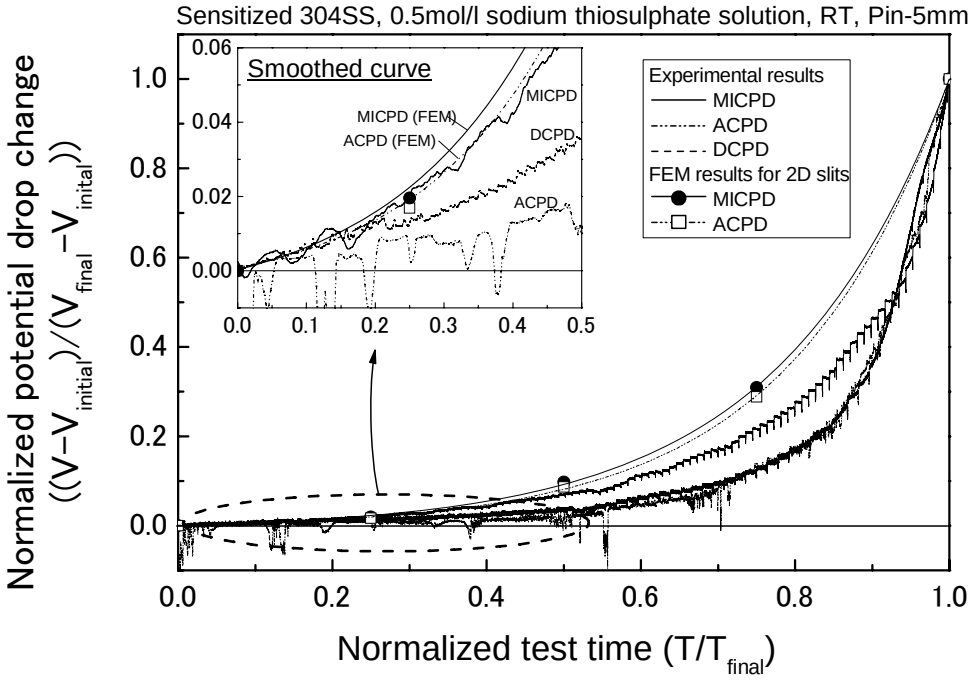

Figure 11 Measured potential drops during the SCC tests.

4. Conclusions

Stress corrosion cracking (SCC) tests, using welded specimens of sensitized type 304 stainless steel with a thickness of 20 mm, were performed under sodium thiosulphate solution at room temperature and continuous monitoring of the SCC growth was performed using the techniques of modified induced current potential drop (MICPD), alternating current potential drop (ACPD) and direct current potential drop (DCPD). The following conclusions can be reached from the results:

(1) The MICPD and DCPD techniques can perform continuous monitoring of back wall SCC, initiating from a fatigue pre-crack at a depth of about 4mm, until it propagates to more than 80% of the specimen thickness.

(2) The MICPD technique can monitor back wall fatigue crack propagation from a depth of about 3mm to 4.3mm.

(3) The MICPD technique can decrease the effect of the current flowing in the direction of the crack length by focusing the induced current into the local area of measurement by using the induction coils, and as the result, the sensitivity of the continuous monitoring of the back wall SCC is higher than that of either of the ACPD or DCPD techniques.

More work is needed to accurately size defect because potential drop techniques generally need calibration curves to convert potential drop data into defect depth. The potential drop data measured during the SCC tests in this study can be used as a calibration curve with converting normalized test time into crack depth.

Acknowledgements

This study was partially performed under the sponsorship of JNES open application project for enhancing the basis of nuclear safety (JNES: Japan Nuclear Energy Safety Organization). This study is also partially supported by the Grant-in Aid for the 21st Century COE Program, "The Exploration of the Frontiers of Mechanical Science Based on Nanotechnology" from the Ministry of Education, Culture, Sports, Science and Technology.

References

[1] Cheng CF. Intergranular stress-assisted corrosion cracking of austenitic alloys in water-cooled nuclear reactors. Journal of Nuclear Materials 1975; 57: 11-33.

[2] Suzuki S, Takamori K, Kumagai K, Ooki S, Fukuda T, Yamashita H, Futami T. Evaluation of SCC morphology on L-grade stainless steels in BWRs. JHPI 2004; 42(4): 12-22.

[3] Thompson CD, Carey DM, Perazzo NL. Effects of hydrogen on electropotential monitoring of stress corrosion crack growth. Proceedings of the Eighth International Symposium on Environmental Degradation of Materials in Nuclear Power Systems – Water Reactors 1997: 366-371.

[4] Kanoh Y, Abe H. Proposal for Nondestructive Evaluation procedure of 3D crack shape by means of electrical potential method. Transactions of the Japan Society of Mechanical Engineers 1992; 58(547): 72-79.

[5] Collins R, Michael DH, Clark R. Measurement of crack depth in a transition weld using ACPD. Review of Progress in Quantitative Nondestructive Evaluation 1992; 11: 545-552.

[6] Shoji T, Kim H. Current status and future prospect of potential drop technique for nondestructive evaluation. The Piping Engineering 1996; 38(1): 51-60.

[7] Kim H, Shoji T. A Study on induced current focusing potential drop (ICFPD) technique - Examination of the sizing accuracy of defects and its frequency dependence -. Journal of The Society of Materials Science Japan 1994; 43(494): 1482-1488.

[8] Kim H, Shoji T. A study on induced current focusing potential drop (ICFPD) technique - Improvement of probe and application for the estimation of 2-dimensional surface defect -. Journal of The Society of Materials Science Japan 1995; 44(500): 669-674.

[9] Sato Y, Takeda Y, Shoji T. Nondestructive evaluation of fatigue and creep-fatigue damage by mans of ICFPD technique. Fatigue & Fracture of Engineering Materials & Structures 2001; 24(12): 885-893.

[10] Cihal V, Shoji T, Kain V, Watanabe Y, Stefec R. EPR - A comprehensive review, 2004.

[11] JSME data book: Fatigue of materials IV - Low cycle fatigue strength, 1983.

[12] Newman JC, Raju IS. An empirical stress intensity factor equation for the surface crack. Engineering Fracture Mechanics 1981; 15: 185-192.

[13] Newman RC, Sieradzki K, Isaacs HS. Stress-corrosion cracking of sensitized type 304 stainless steel in thiosulphate solutions. Metallurgical Transactions A 1981; 13A: 2015-2026.

[14] Cragnolino G, Macdonald DD. Intergranular stress corrosion cracking of austenitic stainless steel at temperatures below 100C – A review, Corrosion 1982; 38(8): 406-424.

Captions

Figure 1 Illustrations of the arrangement of induction coils.

Figure 2 Illustration of the vertical flux sensor (dimensions in mm).

Figure 3 Illustration of the model for the FEM analysis (dimensions in mm).

Figure 4 Current density distributions along the X-axis calculated with FEM (Δ=70mm).

Figure 5 Potential drop distributions measured on the 316SS plate specimen.

Figure 6 Specimen geometry (dimensions in mm).

Figure 7 Illustration of the continuous monitoring system for both the ACPD and MICPD techniques.

Figure 8 The mode of load application for pre-cracking and the SCC test.

Figure 9 Potential drop distribution measured during the fatigue pre-cracking.

Figure 10 Fracture surface with typical IGSCC fractures for the specimen used in the measurements with the MICPD technique.

Figure 11 Measured potential drops during the SCC tests.

Table 1 Combinations of measurement parameters for each sensor.

Table 2 Electromagnetic properties used in the FEM analysis.

Table 3 Detection sensitivity to back wall defects.

Table 4 Chemical composition (wt%) and mechanical properties (room temperature) of the investigated 304SS.

Table 5 TIG welding conditions used for the SCC test specimens.

Table 6 Crack sizes for each test.

Table 7 Measured potential drop without loading condition.